

## VCNC CONTOUR FOLLOWING TASKS USING ROBUST QFT CONTROLLER\*

J. JAHANPOUR<sup>1\*\*</sup>, M. HONARI-TORSHIZI<sup>2</sup> AND M. R. GHARIB<sup>3</sup>

<sup>1,2</sup>Dept. of Mechanical Engineering, Mashhad Branch, Islamic Azad University, Mashhad, I. R. of Iran  
Email: jahanpourfr@mshdiau.ac.ir

<sup>3</sup>Dept. of Mechanical Engineering, Ferdowsi University of Mashhad, Mashhad, I. R. of Iran

**Abstract**– In this paper, the Quantitative Feedback Theory (QFT) is proposed to design a controller for feed drive of Virtual Computer Numerical Control (VCNC) systems. The designed robust QFT controller is also compared to two commonly used controller design methods, i.e. Fuzzy Control (FC) and Sliding Mode Control (SMC), for contour tracking problem. The position commands required for contour following task are evaluated by the Non-Uniform Rational B-Spline (NURBS) curve interpolator with the S-shape feedrate profile for two contours, i.e. "heart" and "omega" as the case studies. After modeling the feed drive of the VCNC system, the robust QFT controller and also FC and SMC controllers are designed to achieve the allowable tolerance contour error. The simulation results for the "heart" and "omega" contour following tasks with the aforementioned controllers were analyzed and discussed. It is found that the designed QFT controller not only achieves the tight contour error but also yields better satisfactory performance, especially at the corners of the tool path, compared to the other controllers used in contour following applications in VCNC systems.

**Keywords**– QFT controller, VCNC, NURBS interpolator, contour tracking, contour error

### 1. INTRODUCTION

Since Bode's work [1] was limited to gain variations only, Horowitz generalized and extended it to arbitrary variations of a process transfer function [2]. He characterized the model uncertainty by templates that are sets of amplitudes and phase for each frequency. Furthermore, a graphical design technique was introduced that was very useful to design feedback systems which were robust to disturbances. QFT is a phrase used to identify the design method Horowitz developed for designing robust control systems. QFT is a robust feedback control-system design technique which allows direct design to closed-loop robust performance and stability specifications. Some advantages of QFT in contrast with other robust control techniques are given in [3-7]:

Trajectory following tasks using the QFT have been considered and implemented in several researches in recent years [7-10]. The main advantage of QFT is its robustness and stability that is against the other defects and allows for the development of a single controller to handle all possible plants defined by the space of uncertainty. Patil et al. [7] proposed a fractional-order proportional-integral (FOPI) controller via the QFT technique for a class of nonlinear systems. In their work, the performance of the designed FOPI controller was also compared with a traditional integer-order PID (IOPID) controller for an arbitrary trajectory as an input. The results presented in [7] showed that in the case of FOPI controller with the QFT technique there was no overshoot in the closed-loop response, whereas large overshoot was

---

\*Received by the editors February 14, 2014; Accepted June 9, 2014.

\*\*Corresponding author

observed in the case of IOPID controller. In [8], the QFT was used for designing controllers for a highly uncertain two link robot manipulator operated in the vertical plane carrying an uncertain payload. In that work, two controllers were designed and their effectiveness was analyzed based on the results obtained from the simulations and experiments. The first one was for tracking a square wave in the presence of plant input and plant output disturbances and the second one was for rejecting random white noise. To control nonlinear vehicle model at different work conditions with eight degrees of freedom, a robust controller based on QFT was used in [9]. In order to reveal the effectiveness of the designed controller, two manoeuvres were considered for the vehicle motions under different working schemes. The results presented in [9] showed that the designed QFT controller with the presence of different uncertainties was able to achieve the accurate desired responses. Amiri Moghadam et al. [10] proposed QFT to control a two-segment robot manipulator along the horizontal line and elliptical trajectories. In fact, the robust control QFT was applied to control the conjugated polymer actuator in their work. The results presented in [10] showed that the designed QFT controller had consistent and robust tracking performance.

Accurate estimation of the contour error is one of the crucial factors in the contour following problems. In fact, several contour-error estimation algorithms that can be used in high speed contouring applications have been proposed [11-14]. Since producing in the shortest time and with the least cost are the main purposes of manufacturing technologies, virtual manufacturing systems provide a useful means for products to be manufactured without the need of physical testing on the shop floor [15]. In particular, Virtual Computer Numerical Control (VCNC) systems have an important role in manufacturing problems and contour error estimation with low cost.

In this paper, the QFT controller is designed for the Non-Uniform Rational B-Spline (NURBS) contour following task in a VCNC system. Due to the fact that the performance of QFT controller has not yet been compared with the other controllers used in VCNCs, in this work, the designed robust QFT controller is also compared with two commonly used controllers in contour following tasks, i.e. Fuzzy Control (FC) and Sliding Mode Control (SMC). The rest of the paper is organized as follows: In Section 2, the VCNC motion control system, which includes the NURBS contouring commands module, the controller and the feed drive dynamics are investigated. In particular, the robust QFT controller design procedure is explained in this section. In Section 3, the simulation results are presented to demonstrate the feasibility of the proposed robust QFT controller for NURBS contour following task in the VCNC. Also, the obtained contouring performance using the designed robust QFT controller is compared with the contouring performance using the FC and SMC controllers in this section. Finally, Section 4 concludes the paper.

## **2. VIRTUAL CNC MOTION CONTROL SYSTEM**

Schematic diagram of a VCNC motion control system is shown in Fig. 1. According to Fig. 1, the VCNC which includes command generation module, controller and feed drive dynamics, is such a system comprising practical models in modelling the real CNC behaviour in assisting the development of a virtual machine tool structure [16].

As shown in Fig. 1, using the designed desired trajectory and the given feedrate profile, the interpolator generates the desired position commands for each axis as the inputs of the system feed drives. The precision of the motion command generator and the designed controller ensure the contouring accuracy of a motion control system [17, 18]. Each part of the VCNC motion control system is described in the following sub-sections.

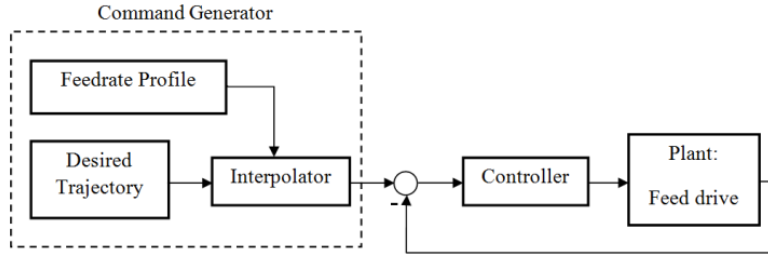


Fig. 1. Schematic diagram of a VCNC motion control system

**a) Feed drive model**

A typical feed drive of a VCNC system is shown in Fig. 2. The linear dynamic model of the feed drive includes the current amplifier, motor gain, inertia and viscous damping, as shown in Fig. 2. The position of the table can be expressed as follows in Laplace domain [19]:

$$X_t(s) = \frac{r_g}{s} \frac{1}{Js + B} [K_t K_a U_a(s) - T_d(s)] \tag{1}$$

where  $u_a$  [V] is the control signal generated by the axis controller and it is applied to the current amplifier which has a gain of  $K_a$  [A/V].  $K_t$  [Nm/A] is the motor torque constant.  $J$  [kg/m<sup>2</sup>] is the inertia of the rigid body motion of the table.  $B$  [kg/m<sup>2</sup>/s] is the system's viscous damping and  $r_g$  [mm/rad] is the transmission gain. The uncertain parameters can be considered as  $B, r_g, K_a,$  and  $K_t$  in the feed drive model of a VCNC system.  $T_d$  [Nm] is the external disturbance torque and consists of non-linear guide way friction  $T_f$  and cutting forces  $T_c$  acting on the motor shaft as  $T_d = T_f + T_c$ .

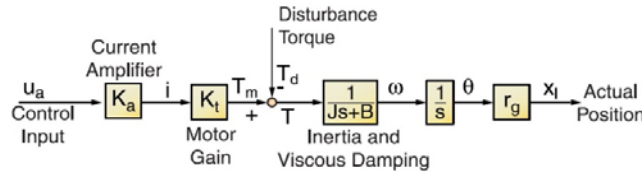


Fig. 2. Feed drive model of a VCNC system [19]

**b) Trajectory command generation module**

Based on the specified feedrate along a tool path designed via a parametric curve, the trajectory command generation module in a VCNC evaluates the curve parameters corresponding to each sampling period and consequently generates the position commands for the drive axes at each sampling period  $T$ . The NURBS curve as the designed tool path and the NURBS interpolator with the S-curve feedrate profile have been used in this paper.

In the following, the NURBS curves and their interpolation using the second-order Taylor's expansion are briefly presented.

1. Review on NURBS curves

The NURBS curve of degree  $p$ , defined by given  $n+1$  control points  $P_0, P_1, \dots, P_n$  with corresponding weights  $w_0, w_1, \dots, w_n$  and the knot vector  $U = \{u_0, u_1, \dots, u_m\}$  is:

$$C(u) = \frac{\sum_{k=0}^n N_{k,p}(u) w_k P_k}{\sum_{i=0}^n N_{i,p}(u) w_i} = \sum_{k=0}^n R_{k,p}(u) P_k \tag{2}$$

where  $R_{k,p}(u)$  and  $N_{k,p}(u)$  are the Rational B-spline and basis functions of degree  $p$ , respectively, which are described as follows [20, 21]:

$$R_{i,p}(u) = \frac{N_{i,p}(u)w_i}{\sum_{j=0}^n N_{j,p}(u)w_j} \quad (3)$$

$$N_{i,0}(u) = \begin{cases} 1 & \text{if } u_i \leq u < u_{i+1} \\ 0 & \text{otherwise} \end{cases}$$

$$N_{i,p}(u) = \frac{u - u_i}{u_{i+p} - u_i} N_{i,p-1}(u) + \frac{u_{i+p+1} - u}{u_{i+p+1} - u_{i+1}} N_{i+1,p-1}(u) \quad (4)$$

The  $m$ -th derivative formula of a NURBS curve defined by equation (2) with respect to the parameter  $u$  is

$$C^{(m)}(u) = \sum_{i=0}^n R_{i,p}^{(m)}(u)P_i \quad (5)$$

where  $R_{i,p}^{(m)}(u)$  is the  $m$ -th derivatives of  $R_{i,p}(u)$ .

Further details on computing the  $m$ -th derivative of a NURBS curve, i.e.  $C^{(m)}(u)$ , specially the first- and the second-order derivatives of a NURBS curve can be found in [20-22].

## 2. NURBS interpolation using the second-order Taylor's expansion

After designing a contour via the NURBS curve as Eq. (2), in order to implement the contour following task, the position commands along the NURBS curve are found using the interpolation technique. To this end, at first the feedrate along the NURBS curve is expressed as

$$V(t) = \frac{ds}{dt} = \frac{ds}{du} \frac{du}{dt} \quad (6)$$

where  $s$  is the arc length. Thus we have

$$\frac{du}{dt} = \frac{V(t)}{\sqrt{\left(\frac{dC_x(u)}{du}\right)^2 + \left(\frac{dC_y(u)}{du}\right)^2}} \quad (7)$$

Where  $C_x(u)$  and  $C_y(u)$  are the  $x$  and  $y$  components of a point on the NURBS curve corresponding to the parameters  $u$ . The closed form solution of Eq. (7) for the NURBS parameter  $u$  does not exist in general. To cope with this problem, the NURBS interpolator is executed using the second-order Taylor's expansion method around the  $t=kT$  instant as:

$$u_{k+1} = u_k + T \frac{du_k}{dt} + \frac{T^2}{2} \frac{d^2u_k}{dt^2} \quad (8)$$

where  $T$  is the sampling period.

The first- and the second- derivatives of  $u(t)$  can be expressed as follows:

$$\frac{du_k}{dt} = \frac{V(t)}{\left\| \frac{d\mathbf{C}(u)}{du} \right\|} \tag{9}$$

$$\frac{d^2u_k}{dt^2} = \frac{\frac{dV(t)}{dt}}{\left\| \frac{d\mathbf{C}(u)}{du} \right\|} - \frac{V^2(t) \left( \frac{d\mathbf{C}(u)}{du} \cdot \frac{d^2\mathbf{C}(u)}{du^2} \right)}{\left\| \frac{d\mathbf{C}(u)}{du} \right\|^4} \tag{10}$$

In the above equations, the first- and second- derivatives of the NURBS curve  $\mathbf{C}(u)$  can be calculated using equation (5). Finally, after obtaining the parameter values from equations (8)-(10), the position commands are calculated by substituting the parameter values into equation (2) at each sampling period.

In order to obtain smooth motion transition between different phases along the path and also ensure continuity of both the feed acceleration/deceleration and feed jerk, the S-curve profiles are preferred rather than the linear one [23]. The cubic time-dependent feedrate used in [22,24] has been adopted for the S-curve feedrate profile in this paper. This feedrate profile consists of three phases of motion as acceleration, fixed feedrate and deceleration. Further details on constructing the feedrate profile can be found in [22-25].

**c) The proposed robust QFT controller for contour following task**

This section presents the QFT controller design procedure for each axis of the VCNC system. The controller designing steps are just illustrated for the x-axis and the controller design for the y-axis has the same procedure.

Figure 3 shows the basic structure of a feedback system with two degrees of freedom. As shown in Fig. 3,  $P(s)$  is uncertain plant that belongs to a set  $P(s) \in \{P(s, \alpha); \alpha \in A\}$ , where  $\alpha$  is the vector of uncertain parameters, which takes the values in  $A$ . Also,  $G(s)$  is the fixed structure feedback controller and  $F(s)$  is the pre-filter. In 2-dof system, it is required to design pre-filter  $F(s)$  and compensator  $G(s)$  for a plant  $P(s)$ .

The uncertain model of the feed drive of the VCNC between the input voltage and output position of the table can be considered as shown below:

$$X_t(s) = \frac{r_g}{s} \frac{1}{J_x s + B_x} [K_t K_{ax} U_a(s) - T_{dx}(s)], \quad Y_t(s) = \frac{r_g}{s} \frac{1}{J_y s + B_y} [K_t K_{ay} U_a(s) - T_{dy}(s)]$$

where the uncertain model's parameters are considered as  $B, r_g, K_a,$  and  $K_t$ . These parameters belong to the following domains for the VCNC system performed in this paper.

$$r_g \in [1.4, 1.73] \text{ mm / rad}, K_t \in [0.42, 0.52] \text{ Nm / A}, K_{ax} \in [5.71, 7.07] \text{ A / V},$$

$$K_{ay} \in [6.67, 8.26] \text{ A / V}, B_x \in [0.014, 0.026] \text{ Kgm}^2 / \text{s}, B_y \in [0.02, 0.037] \text{ Kgm}^2 / \text{s}$$

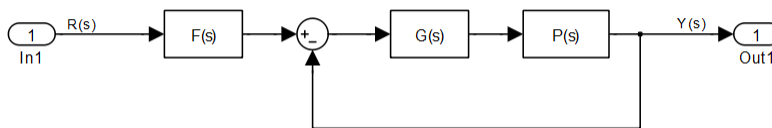


Fig. 3. Structure of a feedback system

Prior to the QFT controller design, the plant templates at specified frequencies that pictorially describe the region of plant parameter uncertainty on the Nichols Chart (NC) should be generated [26, 27]

. To this end, suitable controller and pre-filter must be synthesized such that the closed-loop system is stable and can track the desired position commands as the inputs. Therefore, the following specifications are considered in QFT controller for the VCNC system.

- Robust stability

For a lower gain margin of at least 5.26 dB and a lower phase margin of at least 49.25 deg, the robust stability specification is determined as [28, 29]:

$$\left| \frac{P(j\omega)G(j\omega)}{1+P(j\omega)G(j\omega)} \right| < \mu = 1.2 \quad (11)$$

which corresponds to the lower gain margin of  $K_M = 1 + \frac{1}{\mu} = 1.833 = 5.26$  dB and the lower phase margin of  $\phi_M = 180 - \cos^{-1}(0.5 / \mu^2 - 1) = 49.25$  deg.

- Robust tracking performance

The tracking specifications for the closed-loop performance are given in the form of upper and lower bounds in the frequency domain (overshoot =2% and the settling time =0.05 s). Usually, based on the simple second-order models to represent appropriate under damped and over damped closed-loop system, the following is stated:

$$a(j\omega) < \left| F(j\omega) \frac{P(j\omega)G(j\omega)}{1+P(j\omega)G(j\omega)} \right| < b(j\omega) \quad (12)$$

where,  $a(j\omega)$  and  $b(j\omega)$  are the lower and upper bound, respectively and are  $a(j\omega) = \frac{40000}{s^2 + 400s + 40000}$ ,  $b(j\omega) = \frac{65796}{s^2 + 400s + 65796}$  for the VCNC system.

At the first step of QFT controller design we must define the plant uncertainty (template) on the Nichols Chart, which is shown in Fig. 4. The next step of QFT controller design is the generation of stability contour margin and tracking bounds on the Nichols Chart. Given the plant templates, QFT converts closed-loop magnitude specifications into magnitude and phase constraints on a nominal open loop function  $L_0(s) = G(s)P(s)$  [30]. These constraints are called QFT bounds. Equation (11) established a circle in Nichols chart that also defines phase margin and gain margin. Robust margin bounds (U-contours) are depicted in Fig. 5. The boundary of this region is referred to as the stability bound. For the tracking bounds, the solution requires that the response lie within the upper and lower tracking specification as in equation (12). Robust tracking bounds are shown in Fig. 6. Also, the intersection of the bounds or the robust performance bound is shown in Fig. 7. By considering the frequency constraints and the nominal loop of the system, one can design the controller on the NC by adding poles and zeros and using the QFT toolbox in MATLAB software, so that the open loop transfer function exactly lies on its robust performance bounds and does not penetrate the U-contour at all frequency values ( $\omega_i$ ). The designer performs loop shaping process, which tunes the parameters of controller functions ( $G(s)$ ) until the optimal controller with the minimum high frequency gain is reached without violating the frequency constraints.

Finally, the QFT design can be completed with a pre-filter ( $F(s)$ ) design which guarantees the satisfaction of tracking specification [31]. In the case of tracking conditions, a shaping on the Bode diagram is used. The loop and the pre-filter shaping of the open loop transfer function for the x-axis are presented in Figs. 8 and 9, respectively.

It can be seen that the design satisfies all robust stability margins and the performance specifications. The respected controller and the pre-filter for x- and y- axes are found as follows:

$$G(s) = \frac{22.36s + 61.21}{0.0001s + 1.326}, F(s) = \frac{8.72}{0.001s^2 + 0.187s + 8.72}$$

Once the controller design is finished, the frequency responses of the closed-loop system at several frequencies and time domain simulations must be checked to confirm whether it satisfies the design specifications. Figure 10 illustrates robust stability in frequency domain for the x-axis. Dotted line is the desired stability value ( $\mu=1.2=1.58$  dB) and the continuous line is the system response which is below the dotted line. Also, Fig. 11 shows the time-domain closed-loop response of the associated linear system of VCNC for various plant parameters. According to Figs. 10 and 11, the required robust stability condition for the designed QFT used in the VCNC system is fulfilled.

The performance of the designed QFT controller in the contour following task is also compared with the performances obtained from Fuzzy Control (FC) and Sliding Mode Control (SMC) methods in this paper. The rule bases of the fuzzy controllers for the x and the y axes have also been selected as given in Table 1. The control parameters for the designed SMC are also given in Table 2.

Table 1. Rule base of the fuzzy controllers used in the simulations for both x- and y- axes

		Error						
		NL	NM	NS	Z	PS	PM	PL
Error Change	NL	NL	NL	NL	NL	NM	NS	Z
	NM	NL	NL	NL	NM	NS	Z	PS
	NS	NL	NL	NM	NS	Z	PS	PM
	Z	NL	NM	NS	Z	PS	PM	PL
	PS	NM	NS	Z	PS	PM	PL	PL
	PM	NS	Z	PS	PM	PL	PL	PL
	PL	Z	PS	PM	PL	PL	PL	PL

Table 2. The control parameters for the SMC used in the simulations [19, 32]

SMC parameters	x-axis	y-axis	Unit
Sliding surface bandwidth, $\lambda$	200	200	rad/s
Feedback gain, $K_s$	0.3	0.3	Vs/mm
Disturbance adaptation gain, $\rho$	30	30	V/mm
Lower external disturbance limit, $d^-$	-0.32	-0.54	-
Upper external disturbance limit, $d^+$	0.43	0.58	-

### 3. SIMULATION RESULTS

The x- and the y-axes feed drive parameters used in simulations are given in Table 3. The S-curve feedrate profile with maximum of 100 mm/s and acceleration / deceleration time of 0.12 s is selected for all contour following tasks. In addition, the sampling period  $T$  for the NURBS interpolation is 0.001s in all simulations.

Table 3. The x- and the y-axes feed drive parameters used in the simulations [19, 32]

Feed drive parameters	x-axis	y-axis	Unit
Total reflected inertia, $J$	0.0077736	0.0098109	Kgm <sup>2</sup>
Saturation limits	-5,+5	-5,+5	V
Backlash, $D_b$	0.003	0.003	mm
Static friction, $T_{stat}^{\pm}$	2.6256, -1.8672	2.7658, -2.4520	Nm
Coulomb friction, $T_{cont}^{\pm}$	2.1529, -1.4730	2.5228, -2.3887	Nm

**a) Case studies**

In order to evaluate the performance of the designed controllers, i.e. the QFT, the FC and the SMC in the contour following task, these three controllers were realized for two NURBS curves, i.e. the "heart" and the "omega" shapes, as case studies.

The NURBS parameters for the "heart" shape are:

$$\text{Control points: } \begin{cases} x = [0, 0, -20, 40, 90, 40, -20, 0, 0] \\ y = [0, 10, 50, 50, 0, -50, -50, -10, 0] \end{cases}$$

$$\text{knot vector} = \{0,0,0,0, 1, 2, 3, 4, 5, 6, 6, 6, 6\}, \text{ weights} = [1, 1, 1.7, 1, 4, 1, 1.7, 1, 1], p=3$$

while the parameters for constructing the "omega" shape via the NURBS curve are selected as follows:

$$\text{Control points: } \begin{cases} x = [0, 0, 6, 4, 1, 5, 11, 15, 12, 10, 16, 16] \\ y = [1, 0, 0, 2, 11, 16, 16, 11, 2, 0, 0, 1] \end{cases}$$

$$\text{knot vector} = \{0, 0, 0, 0.025, 0.1, 0.2, 0.4, 0.5, 0.6, 0.8, 0.9, 0.975, 1, 1, 1\}$$

$$\text{weights} = [1, 1, 1, 1, 1, 1, 1, 1, 1, 1, 1, 1], p=2.$$

In the following, the contour following results for the aforementioned case studies are presented.

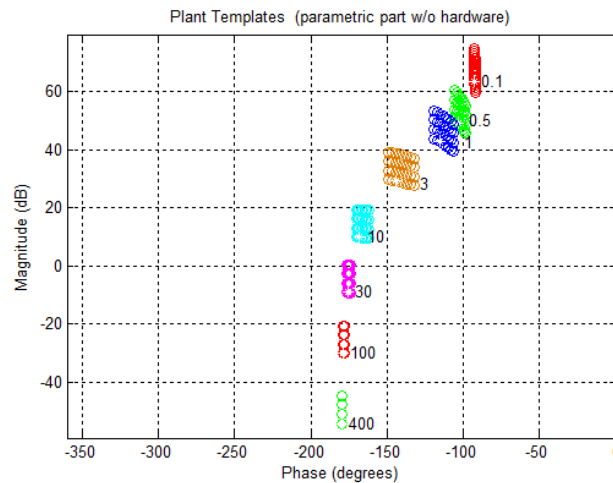


Fig. 4. Boundary of the plant template on the NC

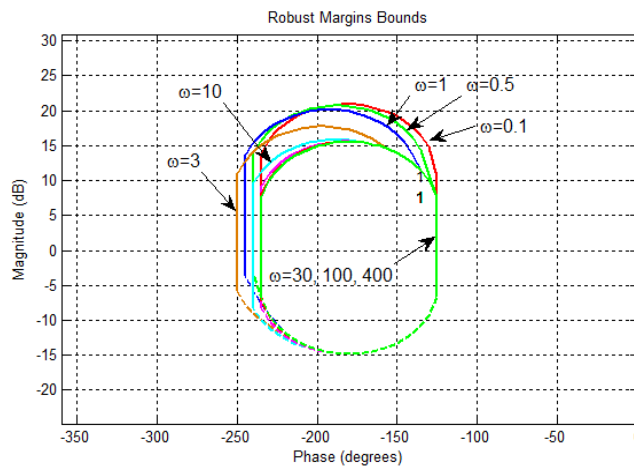


Fig. 5. Robust margins on the NC



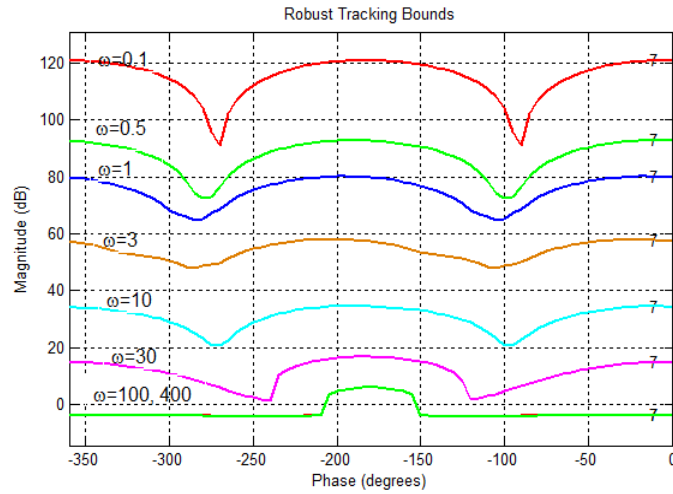


Fig. 6. Robust tracking on the NC

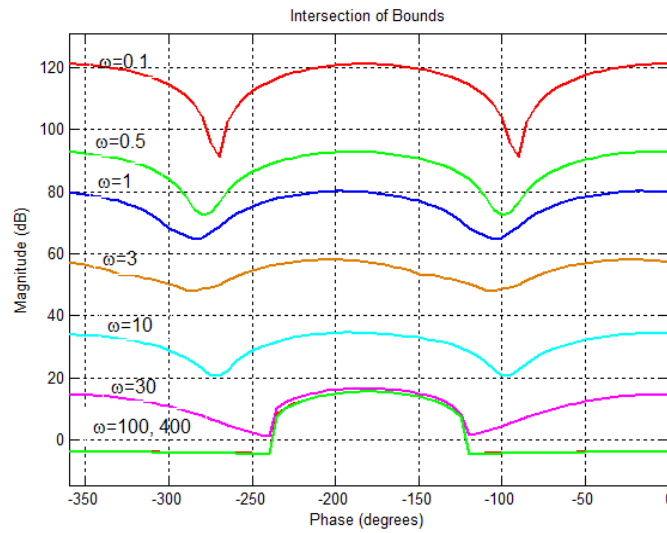


Fig. 7. Intersection of bounds on the NC

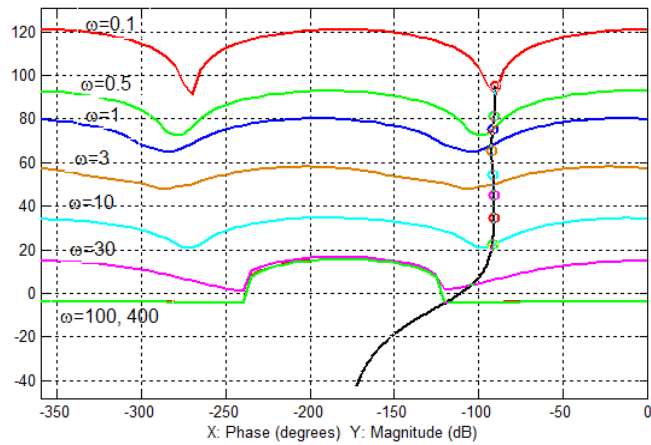


Fig. 8. Loop-shaping in the NC

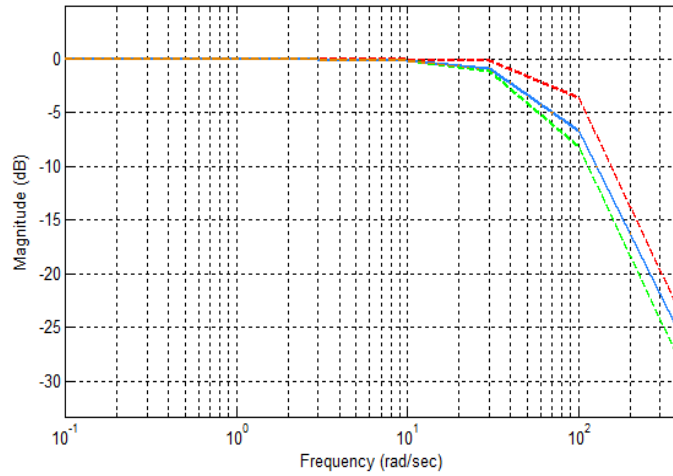


Fig. 9. Pre-filter shaping in the frequency domain

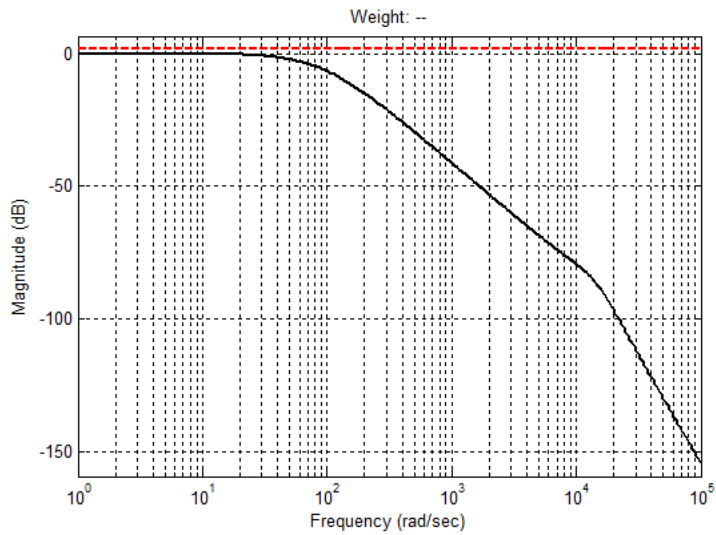


Fig. 10. Robust stability in the frequency domain

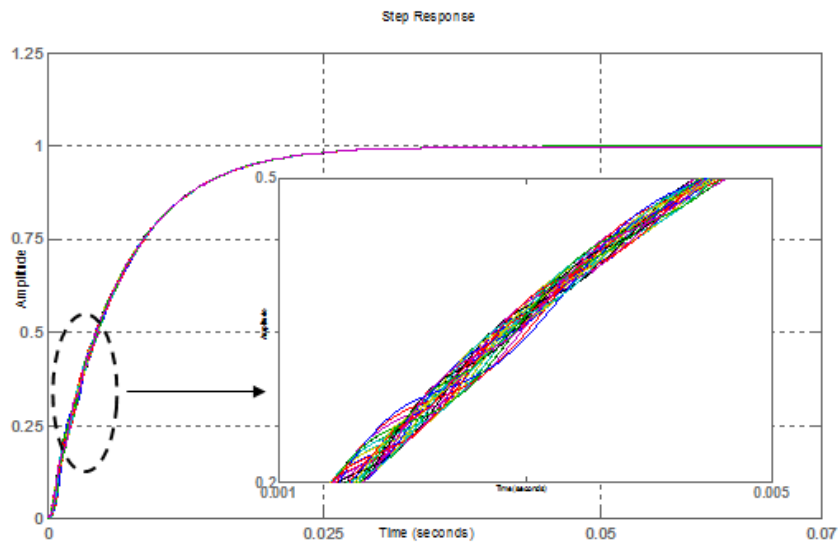


Fig. 11. Closed-loop response of the VCNC system for various plant parameters

**b) "Heart" and "omega" contour following results**

The "heart" contouring starts from the origin and moves in a clockwise direction, while for the case of "omega" contouring, the tool moves from the left to the right side along the "omega".

The simulation results for contour following tasks along the "heart" and the "omega" shapes are given in Figs. 12 and 13, respectively. According to Figs. 12 and 13, it can be observed that the actual trajectories match the desired one closely by employing the three designed controllers, i.e. QFT, FC and SMC.

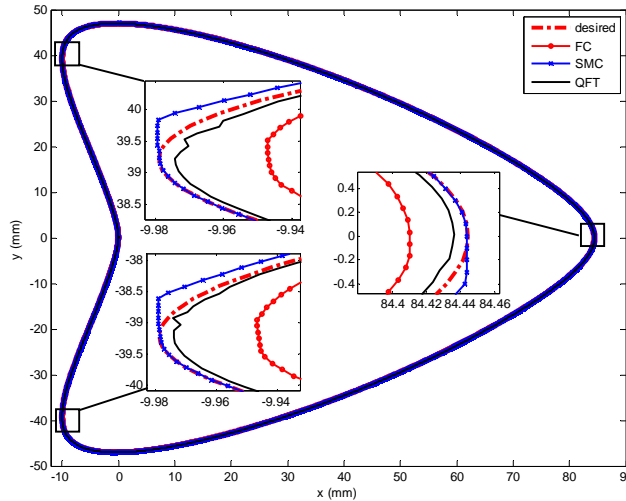


Fig. 12. Contour following performance along the "heart" shaped path

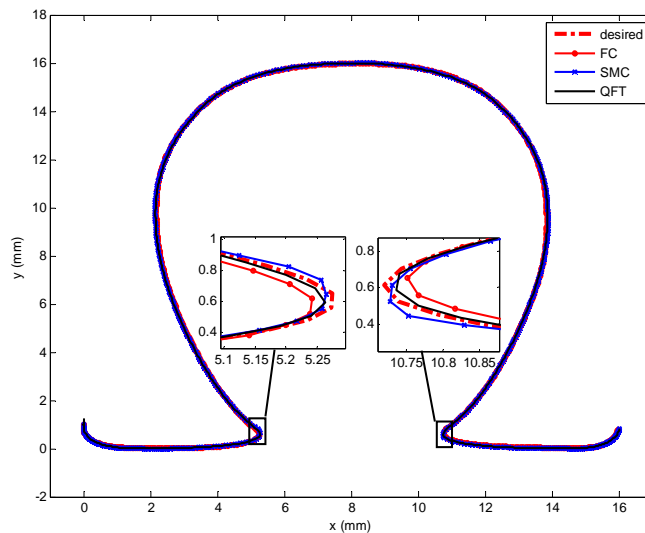


Fig. 13. Contour following performance along the "omega" shaped path

Figure 14 shows the contour error profiles for the "heart" contour following with three designed controllers. While the contour error profiles for the case of "omega" contour following using these controllers are shown in Fig. 15. According to Figs. 14 and 15, the contour error for the "heart" and "omega" contouring is increased in the vicinity of the turning points shown in the insets of Figs. 12 and 13.

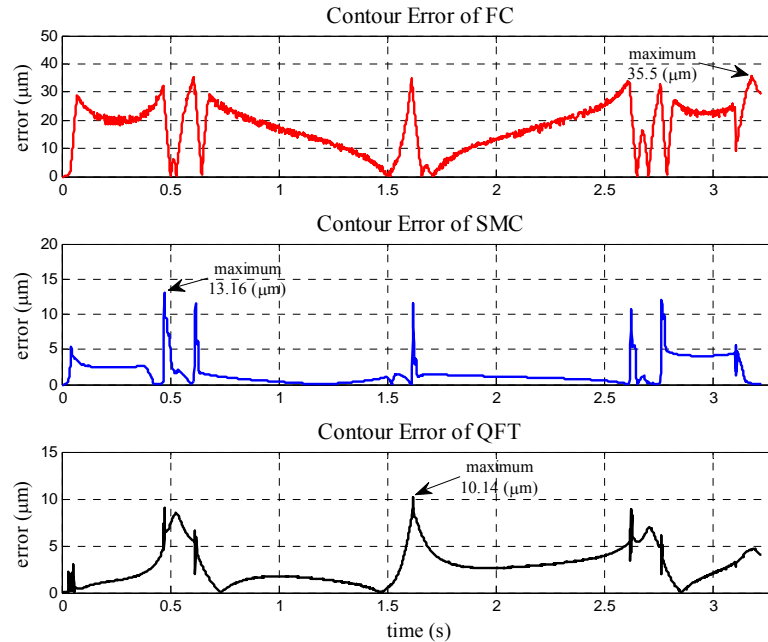


Fig. 14. Contour error of the designed controllers in the "heart" contour following task

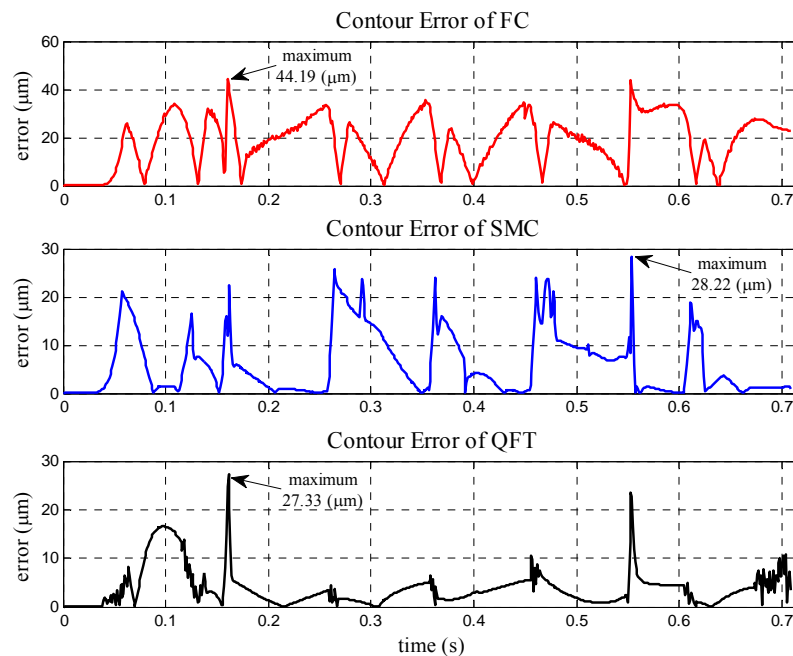


Fig. 15. Contour error of the designed controllers in the "omega" contour following task

For the case of "heart" contour following task, as can be seen in Fig. 14, utilizing the QFT and SMC controllers yields the lower contour error at the corners of the "heart" as the tool path compared with the FC method. The maximum error using the SMC controller occurred at the upper corner of the "heart" is  $13.16 \mu\text{m}$  and the maximum error with the QFT controller is  $10.14 \mu\text{m}$  which occurred at the right-hand side corner of the "heart". However, the "heart" contouring using the FC method yields the contour error more than  $30 \mu\text{m}$  at the turning points and at the end of the tool path as well.

For the case of "omega" contour following task, as can be seen from Fig. 15, the maximum contour

error using the SMC method occurred at the right corner of the "omega" is 28.22  $\mu\text{m}$  and the maximum contour errors using the QFT and FC methods are 27.33  $\mu\text{m}$  and 44.19  $\mu\text{m}$ , respectively, which occur at the left corner of the "omega". Furthermore, the "omega" contouring using the QFT controller not only indicates that the QFT method has least contour error at the corners but also yields the least variation of the contour error at the smooth part between two corners or turning points. Table 4 summarizes the simulation results of the "heart" and "omega" contour following task with three different controllers. The average percentage of contour errors along the "heart" and "omega" paths are also presented in Table 4 for each controller. According to Table 4, the average percentage of the normal distance between the actual tool path and the reference "heart" path using the FC method is 18.54%, which is much more than the other controllers. Also, the average percentage of contouring error along the "omega" path utilizing the designed QFT controller is 6.91%, while the average percentage of contouring error using the SMC and FC methods are 9.46% and 17.82%, respectively.

Table 4. Simulation results for the contour following tasks with the designed controllers

Controller design method	Maximum contour error ( $\mu\text{m}$ )		Average contour error (%)	
	"heart" contour following task	"omega" contour following task	"heart" contour following task	"omega" contour following task
FC	35.5	44.19	18.54	17.82
SMC	13.16	28.22	3.25	9.46
QFT	10.14	27.33	3.34	6.91

#### 4. CONCLUSION

In this paper, design of a robust Quantitative Feedback Theory (QFT) controller for the feed drive of Virtual Computer Numerical Control (VCNC) systems in contour tracking applications was investigated. Also, the performance of the designed robust QFT controller was compared to the performance of fuzzy controller (FC) and sliding mode controller (SMC) for two contour following tasks as the case studies. The position commands required for the contour following tasks were evaluated by the NURBS curve interpolator with the S-curve feedrate planning profile using the second-order Taylor's expansion for two NURBS curves, i.e. "heart" and "omega" shaped path. The simulation results demonstrated that the proposed QFT controller is feasible for tracking the parametric curves represented in the NURBS form. Moreover, it is able to achieve the satisfactory contouring performance, which results in the actual trajectory closely matching the desired path. In particular, utilizing the QFT controller yields the lower contour error at the corners of the tool path compared to the other controller design methods used in VCNC for variable feedrate control.

#### REFERENCES

1. Bode, H. W. (1945). *Network analysis and feedback amplifier design*. Princeton, NJ: Van Nostrand.
2. Horowitz, I. M. (1963). *Synthesis of feedback systems*. New York: Academic Press.
3. Horowitz, I. M. (1992). *Quantitative feedback design theory (QFT)*. 1. 4470 Grinnel Ave., Boulder, Colorado 80303, USA: QFT Publications.
4. Houpis, C. H. & Rasmussen, S. J. (1999). *Quantitative feedback theory fundamentals and application*. New York: Marcel Dekker, Inc.
5. Sobhani, M. & Rafeeyan, M. (2000). Robust controller design for multivariable nonlinear uncertain systems. *Iranian Journal of science and Technology, Transaction B: Engineering*, Vol. 24, No. 3, pp. 345-356.

6. Honari Torshizi, M., Jahanpour, J. & Gharib, M. R. (2011). A new controlling method for trms based on robust approach. *5th International Symposium on Advances in Science & Technology (5th SASTech)*, Mashhad, Iran.
7. Patil, M. D., Nataraj, P. S. V. & Vyawahare, V. A. (2012). Automated design of fractional PI QFT controller using interval constraint satisfaction technique (ICST). *Nonlinear Dynamics*, Vol. 69, pp. 1405–22.
8. Chatlatanagulchai, W., Srinangyam, C. & Siwakosit, W. (2008). Trajectory control of a two-link robot manipulator carrying uncertain payload using quantitative feedback theory. *Journal of Research in Engineering and Technology*. Vol. 5, No. 1, pp. 45-71.
9. Mashadi, B., Goharimanesh, M., Majidi, M. & Gharib, M. R. (2010). Quantitative Feedback Theory controller design for vehicle stability enhancement. Proceedings of the ASME 2010 10th Biennial Conferences on Engineering Systems Design and Analysis (ESDA2010); 2010 July 12-14; Istanbul, Turkey
10. Amiri Moghadam, A. A., Moavenian, M. & Toussi, H. E. (2011). Modelling and robust control of a soft robot based on conjugated polymer actuators. *International Journal of Modelling Identification and Control*. Vol. 14, No. 3, pp. 216–26.
11. Cheng, M. Y., Su, K. H. & Wang, S. F. (2009). Contour error reduction for free-form contour following tasks of biaxial motion control systems. *Robotics and Computer-Integrated Manufacturing*, Vol. 25, No. 2, pp. 323–33.
12. Erkorkmaz, K., Yeung, C. H. & Altintas, Y. (2006). Virtual CNC System. Part II. High speed contouring application. *International Journal of Machine Tools and Manufacture*. Vol. 46, No. 10, pp. 1124-38.
13. Cheng, M. Y. & Lee, C. C. (2007). Motion controller design for contour following tasks based on real-time contour error estimation. *IEEE T Ind. Electron.*, Vol. 54, No. 3, pp. 1686–95.
14. Erkorkmaz, K. & Altintas, Y. (1998). High speed contouring control algorithm for CNC machine tools. *Proceedings of ASME Dynamic Sys Control Division, IMECE'98, DSC-64*, pp. 463–469.
15. Altintas, Y., Brecher, C., Weck, M. & Witt, S. (2005). Virtual machine tool. *Annals of CIRP*, Vol. 54, No. 2, pp. 651-73.
16. AbdulKadir, A., Xu, X. & Hammerle, E. (2011). Virtual machine tools and virtual machining-A technological review. *Robotics and Computer-Integrated Manufacturing*, Vol. 27, pp. 494–508.
17. Erkorkmaz, K. & Altintas, Y. (2001). High speed CNC system design. Part I: jerk limited trajectory generation and quintic spline interpolation. *International Journal of Machine Tools & Manufacture*. Vol. 41, pp. 1323-45.
18. Su, K. H. (2008). *Study on contour error control in parametric free-form contour following*. Taiwan, R.O.C.: National Cheng Kung University.
19. Yeung, C. H., Altintas, Y. & Erkorkmaz, K. (2006). Virtual CNC system. Part I. System architecture. *International Journal of Machine Tools and Manufacture*. Vol. 46, pp. 1107–23.
20. Piegl, L. A. & Tiller, W. (1995). *The NURBS Book*. New York: Springer.
21. Shene, C. K. (2011). Introduction to computing with geometry notes. [Internet] Houghton, Michigan: Michigan Technological University. Available from: <http://www.cs.mtu.edu/~shene/COURSES/cs3621/NOTES/>; [updated 2011 May 4].
22. Jahanpour, J., Tsai, M. C. & Cheng, M. Y. (2010). High speed contouring control with NURBS-based  $C^2$  PH spline curves. *International Journal of Advanced Manufacturing Technology*, Vol. 49, Nos. 5-8, PP. 663-74.
23. Tsai, Y. F., Farouki, R. T. & Feldman, B. (2001). Performance analysis of CNC interpolators for time-dependent feed rates along PH curves. *Computer Aided Geometric Design*. Vol. 18, No. 3, pp. 245-65.
24. Jahanpour, J. & Ghadirifar, A. (2014). The improved NURBS-based  $C^2$  PH spline curve contour following task with PDFF controller. *International Journal of Advanced Manufacturing Technology*. Vol. 70, pp. 995-1007.
25. Jahanpour, J. (2012). High speed contouring enhanced with  $C^2$  PH quintic spline curves. *Scientia Iranica B*, Vol. 19, No. 2, pp. 311–31.
26. Amiri Moghadam, A. A., Gharib, M., Moavenian, M. & Torabi, K. (2009). Modelling and control of a SCARA robot using quantitative feedback theory. *Proc IMechE Part I: Journal of Systems and Control Engineering*, Vol. 223, pp. 919–28.

27. Nataraj, P. S. V. (2002). Computation of QFT bounds for robust tracking specifications. *Automatica*, Vol. 38, pp. 327-34.
28. Satpati, B., Koley, C. & Datta, S. (2014). Robust PID controller design using PSO enabled automated QFT approach for first order lag system with minimal dead time. *Systems Science & Control Engineering*. DOI: 10.1080/21642583.2014.912570.
29. Alavi, S. M. M., Izadi-Zamanabadi, R. & Hayes, M. J. (2007). On the generation of a robust residual for closed-loop control systems that exhibit sensor faults. *IET Proc. Irish Signals and Systems Conference N.*, Ireland, pp. 59–66.
30. Borghesani, C., Chait, Y. & Yaniv, O. (1993). *QFT frequency domain control design toolbox; for use with MATLAB*. Terasoft, Inc.
31. Yaniv, O. (1998). *Quantitative feedback design of linear and non-linear control systems*. Kluwer Academic Publication, Norwell, Massachusetts.
32. Altintas, Y., Erkorkmaz, K. & Zhu, W. H. (2000). Sliding mode controller design for high speed drives. *Annals of CIRP*, Vol. 49, No. 1, pp. 265–70.